

Circular RNA circDNA2 upregulates *CCDC6* expression to promote the progression of gastric cancer via miR-149-5p suppression

Duochen Jin,^{1,2,3} Keting Huang,^{1,2,3} Lei Peng,¹ Ping Xu,¹ Yini Dang,¹ Jiajia Yang,¹ Meihong Chen,¹ Xudong Zhu,^{1,2} Shuchun Wei,^{1,2} Jin Yan,^{1,2} and Guoxin Zhang^{1,2}

¹Department of Gastroenterology, First Affiliated Hospital of Nanjing Medical University, No. 300 of Guangzhou Road, Nanjing 210029, China; ²First Clinical Medical College of Nanjing Medical University, Nanjing, China

Circular (circ)RNAs are widely involved in gastric cancer (GC) pathogenesis, and coiled-coil domain containing 6 (*CCDC6*) is a fused partner of multiple oncogenes; however, the underlying mechanisms of how circRNAs regulate *CCDC6* expression in the progression and prognosis of GC remain unclear. Here, we discovered the circRNA derived from the *DNA2* gene locus (circDNA2) through RNA sequencing. By performing quantitative real-time PCR and fluorescence *in situ* hybridization (FISH) assays with a human tissue microarray, circDNA2 was found to be highly expressed in GC tissues and associated with lymphatic invasion of GC patients. Knockdown of circDNA2 expression suppressed the proliferation of GC cells by reducing *CCDC6* expression. Mechanistically, circDNA2 acted as a microRNA (miR)-149-5p sponge, which was confirmed to target *CCDC6* by RNA pulldown and dual-luciferase reporter assays and rescue experiments. Both low miR-149-5p expression and high *CCDC6* expression were related to unfavorable prognosis in GC patients. Moreover, GC patients with low miR-149-5p expression had shorter overall survival and a higher risk of chemotherapy resistance than those with high miR-149-5p expression. In summary, circDNA2 contributes to the growth and lymphatic metastasis of GC by upregulating *CCDC6* expression by sponging miR-149-5p. The circDNA2/miR-149-5p/*CCDC6* axis might be developed as a therapeutic target and prognostic indicator for GC.

INTRODUCTION

Gastric cancer (GC) is the fifth most common malignancy and the third leading cause of cancer-related death worldwide, with an estimated 782,685 GC-related deaths in 2018.¹ Early diagnosis is essential for treating GC patients and thereby improving their prognosis.² However, the early stage of GC lacks specific symptoms, and the diagnosis of GC mainly depends on endoscopy combined with tissue biopsy, imaging examination, and serum tumor marker detection.³ Tissue biopsy is the gold standard method, but this obvious visual change in histopathology is lagging. We hope to identify novel biomarkers closely related to the tumorigenesis of GC that can assist clinicians

in the early risk assessment, individualized treatment, and prediction of survival time of GC.

Circular (circ)RNAs are stable and conserved products of the RNA backsplicing process and are also predominant transcripts of diverse human cell types.^{4,5} circRNAs with covalently closed loop structures are noncoding RNAs (ncRNAs) that facilitate circularization by forming lariat structures or pairing flanking ALU sequences in bordering introns.^{6,7} circRNAs participate in the pathogenesis of many diseases, including cancers, and have been reported to regulate gene expression at the transcriptional, post-transcriptional, and translational levels.^{8,9} Current studies have revealed that circRNAs can promote or inhibit GC initiation and progression by sponging microRNAs (miRNAs) through their miRNA-binding sites.^{10,11} In addition, circRNAs have higher stability and tissue specificity than other ncRNAs, and they are widely distributed in body fluids. Therefore, these molecules may be used as potential GC-related molecular biomarkers or targets for early diagnosis and effective therapy.

Coiled-coil domain containing 6 (*CCDC6*) was originally recognized as a partner in fusion with the tyrosine kinase rearranged during transfection (*RET*) receptor from a human papillary thyroid carcinoma (PTC) sample.¹² The 65 kDa protein product of the *CCDC6* gene is expressed in both the nucleus and cytoplasm of almost all human tissues. To date, *CCDC6* has been identified as a partner of various proto-oncogenes in fusions, such as *MYC*, *MLL3*, *RARA*, *ALK*, and *RUNX1*, other than *RET* in different tumor types, and most of these oncogenes fused to *CCDC6* enhance cell proliferation.¹³

Received 11 November 2020; accepted 26 May 2021;
<https://doi.org/10.1016/j.omtn.2021.05.021>.

³These authors contributed equally

Correspondence: Jin Yan, Department of Gastroenterology, First Affiliated Hospital of Nanjing Medical University, No. 300 of Guangzhou Road, Nanjing 210029, China.

E-mail: jsyj0220@163.com

Correspondence: Guoxin Zhang, Department of Gastroenterology, First Affiliated Hospital of Nanjing Medical University, No. 300 of Guangzhou Road, Nanjing 210029, China.

E-mail: guoxinz@njmu.edu.cn

Fusion of the coiled-coil domain of *CCDC6* to the tyrosine kinase domain of *RET* was identified as a novel oncogenic driver in advanced colorectal cancer.¹⁴ Moreover, as a *ROS1* fusion protein, *CCDC6* promotes oncogenic receptor tyrosine kinase dimerization and activation, which may occur in gastric carcinoma.¹⁵

At present, some studies have explored the regulation of *CCDC6* by a set of ncRNAs. Jia et al. and Leone et al. separately reported that overexpression of miRNA (miR)-146b-5p and miR-130b-3p promoted the development of human thyroid papillary carcinomas and follicular adenomas by both targeting *CCDC6*.^{16,17} A common G/C polymorphism in pre-miR-146a decreased the amount of mature miR-146a, led to reduced inhibition of *CCDC6* gene expression, and genetically predisposed patients to PTC.¹⁸ The miR-19b-3p/*CCDC6* axis was found to enhance cell proliferation and the nuclear translocation of β -catenin to promote intrahepatic cholangiocarcinoma progression *in vivo*.¹⁹

In the present study, we first investigated the correlation of *CCDC6* expression with the clinicopathological characteristics of GC patients and examined the change in *CCDC6* expression from the perspective of ncRNAs in GC progression.

RESULTS

circRNA profiling in GC tissues and circDNA2 characterization

We constructed a circRNA profiling database by sequencing ribosomal RNA-depleted total RNA obtained from tumor tissues and pair-matched adjacent normal tissues of 3 GC patients. The bioinformatics analysis pipeline used to identify candidate circRNAs is summarized in Figure 1A. We detected 3,120 circRNAs in the aforementioned 3 pairs of GC tissues that had been reported on the circBase website. The predicted sequence length of 83.62% (2,609/3,120) of the circRNAs was shorter than 1,000 nucleotides (Figure 1B), which was similar to a previously published study.²⁰ Our RNA sequencing (RNA-seq) data also revealed that 95.96% (2,994/3,120) of the circRNAs were derived from exons (Figure 1C). Twenty-one circRNAs with downregulated expression and ten with upregulated expression in GC tissues were identified as differentially expressed circRNAs by analyzing the cluster heatmap, which shows the expression variations of circRNA transcripts among GC tissues and paired adjacent noncancerous tissues (fold change > 2, $p < 0.05$; Figure 1D). The raw sequencing data were submitted to the Gene Expression Omnibus database (GSE167512). Then, we further detected the expression level of circDNA2 in 20 pairs of GC tissues and matched adjacent normal tissues via quantitative real-time PCR and found that circDNA2 had a higher expression level in tumor tissues ($p < 0.05$; Figure 1E). Compared with that in the immortalized normal gastric epithelial cell line GES-1, the expression of circDNA2 in the GC cell lines AGS, SGC-7901, and BGC-823 was considerably increased, with the highest expression of circDNA2 in AGS GC cells, followed by SGC-7901 GC cells (Figure 1F).

circDNA2 is derived from the DNA replication helicase/nuclease 2 (*DNA2*) gene, which is located at chromosome 10q 21.3, and connects

exon 2 to exon 5 of the *DNA2* gene (chr10:70218860–70229920) to form a circular structure. The genomic sequence length of circDNA2 is 11,060 nt, and its spliced length is predicted to be 645 nt, as shown by the online website circBase (<http://www.circbase.org/>). The head-to-tail splicing structure of circDNA2 was confirmed with quantitative real-time PCR products by Sanger sequencing (Figure 2A). The results of quantitative real-time PCR assays showed that compared with that in the absence of RNase R exonuclease, the relative expression of *GAPDH* in AGS cells decreased by 93.4-fold, linear *DNA2* by 45.0-fold, and circDNA2 by 1.4-fold, indicating that the ability of circDNA2 to tolerate RNase R exonuclease digestion was 32 times that of the homologous linear gene *DNA2*; similar results were obtained in the SGC-7901 GC cells: circDNA2 was 38 times more resistant to digestion induced by RNase R exonuclease than linear *DNA2* gene, suggesting that circDNA2 harbors a nonlinear circular structure (Figure 2B). We next examined the stability of circDNA2 with 2 mg/mL actinomycin D, a transcription inhibitor. Quantitative real-time PCR assays showed that the half-life of the circDNA2 transcript exceeded 24 h, while that of the homologous linear gene *DNA2* was only ~6 h (Figure 2C), suggesting that highly stable circDNA2 has potential as a diagnostic or prognostic biomarker. Furthermore, we analyzed the subcellular localization of circDNA2 and the expression level in GC tissues. Cytoplasmic and nuclear RNAs of AGS and SGC-7901 cells were separately detected by quantitative real-time PCR, and the results showed that circDNA2 was mainly localized in the cytoplasm of the two cell lines (Figure 2D). In addition, we directly observed the localization of circDNA2 in GC tissue cells and adjacent normal tissue cells by fluorescence *in situ* hybridization (FISH). We found that the green fluorescence representing the distribution of circDNA2 was located in the cytoplasm of the two types of tissue cells and that the expression of circDNA2 in GC tissue cells was higher than that in normal tissue cells (Figure 2E). In summary, circDNA2 is a highly stable circRNA localized in the cytoplasm that deserves exploration for its relationship with the diagnosis and prognosis of GC.

CCDC6 increased microsatellite instability and led to an unfavorable prognosis in GC patients

We first analyzed the human GC data in the The Cancer Genome Atlas (TCGA) RNA-seq database combined with normal gastric data from the GTEx V8 database and found that *CCDC6* expression was significantly increased in GC tissues relative to adjacent normal gastric tissues (Figure 3A; Figure S1). We further detected *CCDC6* mRNA expression in 20 GC tissues and paired normal gastric tissues and found that *CCDC6* was highly expressed in the tumor tissues (Figure 3B). We continued to explore the correlation of *CCDC6* expression level with clinicopathological characteristics or prognosis of GC patients in the TCGA database. As shown in Figure 3C, there was a significantly positive correlation of *CCDC6* gene expression levels with the microsatellite instability (MSI) score of the GC patients ($p = 0.016$, $\rho = 0.12$, 95% CI 0.02–0.23, $n = 374$). However, the expression level of *CCDC6* was not significantly correlated with the age, sex, pathological stage, tumor size, T classification, N classification, distant metastasis, or pathological grade of the GC patients (Figures S2A–S2H).

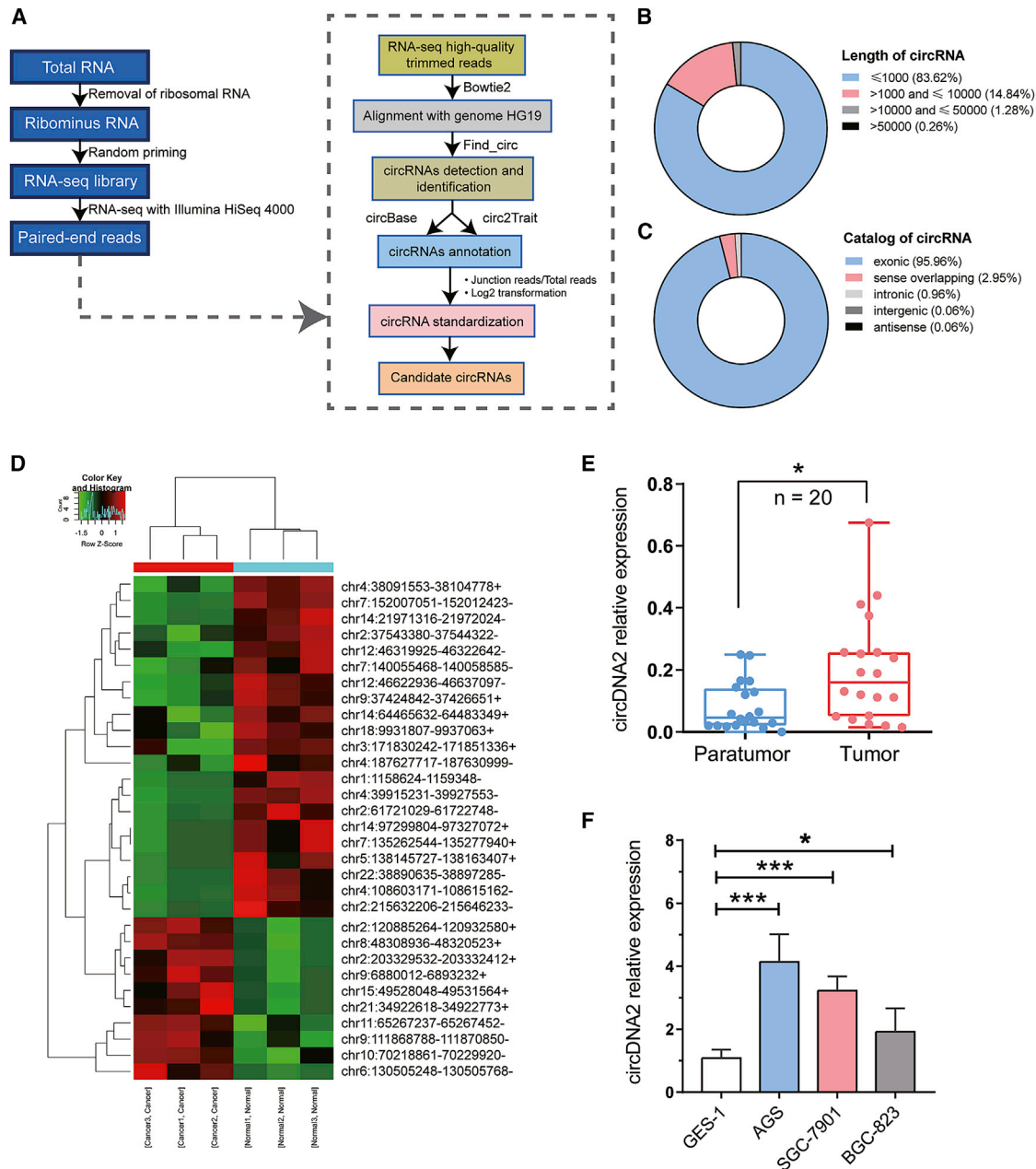


Figure 1. Identification of circDNA2 in the circRNA sequencing database, GC tissues and their paired adjacent normal gastric tissues, and GC cells

(A) The bioinformatics analysis pipeline used to identify candidate circRNAs obtained from RNA-seq reads. (B) The predicted sequence length of circRNAs in the circRNA sequencing database. (C) Gene distribution of circRNA composition in the circRNA sequencing database. (D) The cluster heatmap showed 31 differentially expressed circRNA transcripts (fold-change cutoff > 2, $p < 0.05$) in GC tissues compared with matched normal tissues. (E) The relative expression level of circDNA2 in 20 pairs of GC tissues and adjacent normal gastric tissues (quantitative real-time PCR). (F) Relative expression levels of circDNA2 in GES-1 cells and AGS, SGC-7901, and BGC-823 GC cells (quantitative real-time PCR). The data are represented as the mean \pm SEM. * $p < 0.05$, ** $p < 0.01$, *** $p < 0.001$.

The online platform Kaplan-Meier plotter²¹ was used to estimate the correlation of *CCDC6* expression with overall survival (OS) of GC patients. We found shorter OS and survival after chemotherapy in GC patients with high *CCDC6* expression (Figures 3D and 3I). Further

pathological staging analysis revealed that GC patients with stage II, stage III, or stage IV disease with high *CCDC6* expression had a significantly shorter OS than those with low *CCDC6* expression (Figures 3E–3H).

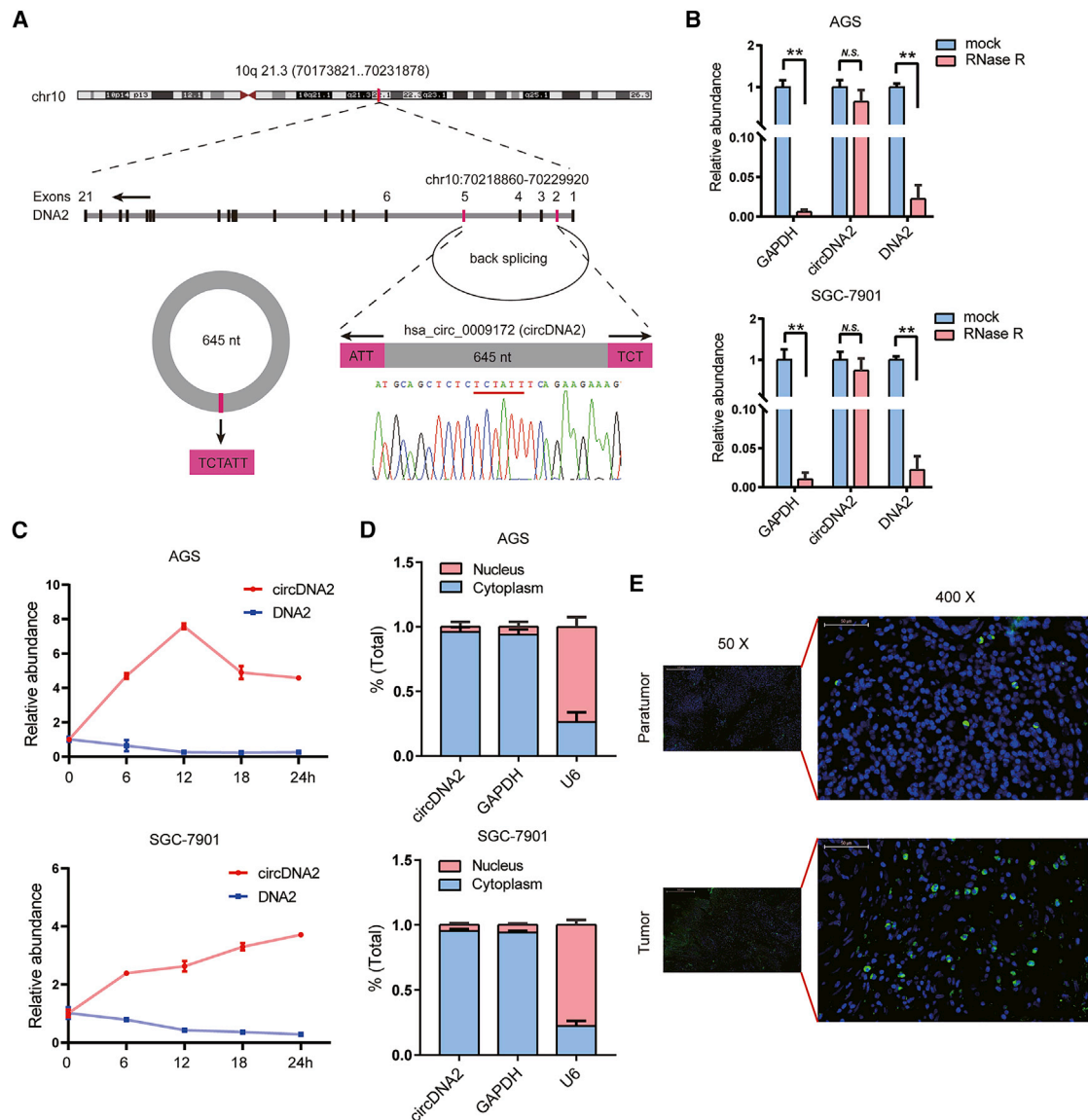


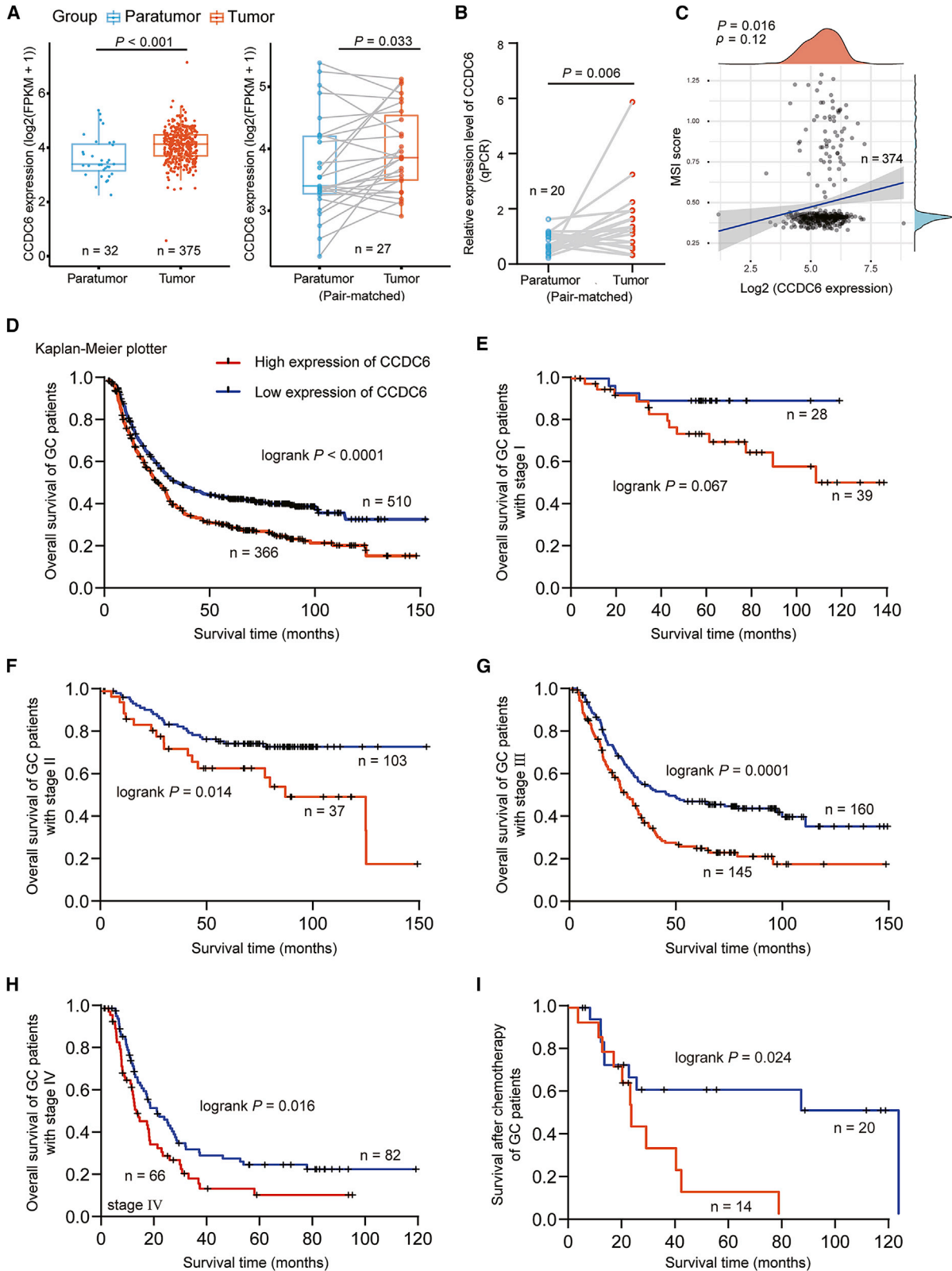
Figure 2. Characterization of circDNA2 in GC tissues and cell lines

(A) We used the UCSC Genome Browser to identify the genomic loci of the *DNA2* gene and circDNA2. The quantitative real-time PCR product of circDNA2 was used to perform Sanger sequencing, indicating that circDNA2 forms a circular structure by head-to-tail splicing. (B) We performed quantitative real-time PCR assays of *GAPDH* RNA, linear *DNA2* RNA, and circDNA2 with or without RNase R digestion in AGS and SGC-7901 GC cells. (C) Relative expression levels of circDNA2 and linear *DNA2* were determined by quantitative real-time PCR assays after actinomycin D treatment at successive intervals of time in AGS and SGC-7901 GC cells. (D) Cytoplasmic and nuclear RNAs of AGS and SGC-7901 GC cells were separately detected by quantitative real-time PCR to identify the subcellular localization of circDNA2. *GAPDH* and *RNU6-1* were used as positive controls for cytoplasmic and nuclear RNAs, respectively. (E) FISH assays were performed to assess the subcellular localization of circDNA2 and its relative expression levels in GC tissue cells and adjacent normal tissue cells. The nuclei were stained blue by DAPI, and circDNA2 was stained green. The scale bar on the left represents 500 μm , and the scale bar on the right represents 50 μm . The data are represented as the mean \pm SEM. * $p < 0.05$, ** $p < 0.01$, *** $p < 0.001$.

miR-149-5p, a potential miRNA that acts as a circDNA2 sponge, may target the *CCDC6* gene

Previous studies have revealed that miRNAs can repress mRNA translation or directly cleave their mRNA targets and thus play pivotal roles in GC occurrence and development.^{22,23} Therefore, we used starBase v.3.0²⁴ (<http://starbase.sysu.edu.cn/index.php>) to verify the potential

miRNAs targeting *CCDC6* gene 3' UTR under strict screening conditions. All miRNAs were expressed in at least 4 tumor types with a strict stringency (≥ 5) for the *CCDC6* gene, which could be predicted in both microT²⁵ and PITA²⁶ target-predicting programs. Next, given that numerous studies indicate that circRNAs sponge and bind to miRNAs to regulate gene transcription and therefore are involved in



(legend on next page)

tumorigenesis,²⁷ we utilized the Circular RNA Interactome²⁸ (https://circinteractome.nia.nih.gov/mirna_target_sites.html) to predict the miRNAs that could be sponged by circDNA2. Fifty-three miRNAs could target the 3' UTR of the *CCDC6* gene, and circDNA2 acted as a miRNA sponge for a total of 31 miRNAs. We took the intersection of the two miRNA collections and screened out two miRNAs that not only could target the *CCDC6* gene 3' UTR but also could bind to circDNA2, hsa-miR-149-5p and hsa-miR-375 (Figure 4A). We further found that miR-149-5p expression displayed a significant negative correlation with *CCDC6* (coefficient $R = -0.255$, $p < 0.0001$) in gastric adenocarcinoma (GAC) tissues (Figure 4B). Therefore, we further observed the expression level of miR-149-5p and its correlation with *CCDC6* expression in the TCGA RNA-seq database and found that the miR-149-5p expression level in GAC tissues was significantly lower than that in adjacent normal tissues ($n = 389$ and 41 , $p < 0.0001$) or pair-matched normal tissues ($n = 41$ and 41 , $p = 0.0034$) and was also negatively correlated with *CCDC6* expression (Figures 4C and 4D).

After we used the Circular RNA Interactome tool to predict the potential binding site of circDNA2 and miR-149-5p (Figure 4E), we conducted a dual-luciferase reporter assay to verify whether the two molecules could directly bind to each other. We inserted the constructed circDNA2 fragment downstream of the luciferase reporter gene. The luciferase reporter gene was then cotransfected with miR-149-5p mimic or inhibitor into AGS or SGC-7901 cells. Compared with cotransfection with the negative control (NC), the miR-149-5p mimic decreased luciferase reporter activity, while the miR-149-5p inhibitor increased the luciferase signal. However, when we next mutated the binding site in the circDNA2 sequence and cotransfected mutant circDNA2 with miR-149-5p mimic or inhibitor into the two cell lines, there were no significant changes in luciferase reporter activity compared with that of the NC group (Figure 4F). The results of RNA pulldown assays showed that circDNA2 and miR-149-5p were prominently enriched in circDNA2-specific probe pulldown samples compared with negative probe pulldown samples in AGS and SGC-7901 cells, which also confirmed the direct binding of miR-149-5p to circDNA2 (Figures 4G and 4H). Moreover, we performed a FISH assay in GC tissue cells to visually observe the direct interaction between circDNA2 and miR-149-5p and found that the two molecules were colocalized in the cytoplasm (Figure 4I). We subsequently found that circDNA2 overexpression or knockdown negatively regulated the expression level of miR-149-5p in AGS or SGC-7901 GC cells, while both the miR-149-5p mimic and inhibitor had no effects on circDNA2 expression, as shown by quantitative real-time PCR (Figure 4J). Finally, we verified the relative expression levels of circDNA2 and

miR-149-5p and their correlation in a human tissue microarray with 80 pairs of matched GC tissues. Since the tissues at 2 sites were missing during the FISH assays (D13 and J3), 78 pairs of GC matched tissues were included for further investigation (Figure 4K). We also discovered that circDNA2 expression was relatively high whereas miR-149-5p expression was low in GAC tissues compared with normal tissues adjacent to the tumor, which were negatively correlated with each other ($r = -0.1925$, $p < 0.05$; Figures 4L and 4M).

miR-149-5p was confirmed to target the *CCDC6* gene

We first found that compared with that in the GES-1 cell line, miR-149-5p expression was low in the AGS and SGC-7901 GC cell lines, while *CCDC6* expression was high in GC cells, as shown by quantitative real-time PCR detection, and miR-149-5p expression in AGS cells was relatively lower than that in SGC-7901 cells (Figure 5A). Therefore, miR-149-5p mimic (60 μ M) was transfected into AGS cells with high circDNA2 expression, and miR-149-5p inhibitor (80 μ M) was transfected into SGC-7901 cells with low circDNA2 expression. Quantitative real-time PCR and western blot assays indicated that miR-149-5p expression increased and *CCDC6* expression decreased 48 h after AGS cells were transfected with miR-149-5p mimic ($p < 0.001$, $p < 0.01$; Figure 5B), while decreased miR-149-5p expression accompanied by increased *CCDC6* expression was detected in the SGC-7901 cells transfected with miR-149-5p inhibitor ($p < 0.001$, $p < 0.001$; Figure 5C). Furthermore, AGS and SGC-7901 cells were cotransfected with miR-149-5p mimic or inhibitor and luciferase reporter vectors including wild-type (WT) or mutant-type (Mut) *CCDC6* 3' UTR (Figure 5D). Consequently, the luciferase activity of the AGS cells with cotransfection of WT *CCDC6* 3' UTR and miR-149-5p mimic was notably decreased ($p < 0.001$; Figure 5E) compared with that of the mimic NC group, but the luciferase activity of the SGC-7901 cells with cotransfection of Mut *CCDC6* 3' UTR and miR-149-5p inhibitor was strongly increased compared with that of the inhibitor NC group ($p < 0.001$; Figure 5F). Interestingly, the luciferase activity of the group with cotransfection of Mut *CCDC6* 3' UTR and miR-149-5p inhibitor was not different from that of the inhibitor NC group ($p > 0.05$), but the luciferase activity of the group cotransfected with Mut *CCDC6* 3' UTR and miR-149-5p mimic was also decreased compared with that of the mimic NC group ($p < 0.001$), which might be due to the residual binding sites of Mut *CCDC6* 3' UTR and miR-149-5p.

Knockdown of circDNA2 reduced *CCDC6* expression and inhibited the proliferation of GC cells *in vitro*

Before exploring the regulatory effects of circDNA2 on *CCDC6*, we first designed an overexpression vector and a small interfering

Figure 3. *CCDC6* increased microsatellite instability and unfavorable prognosis in GC patients

(A) Analysis of the relative expression levels of *CCDC6* in human GC and adjacent normal tissues of TCGA sequencing database (Wilcoxon test and paired Wilcoxon test). (B) *CCDC6* expression was also upregulated in our collected GC tissues compared with the paired adjacent noncancerous tissues by qPCR analysis. (C) We conducted Spearman's correlation analysis to describe the correlation of *CCDC6* gene expression levels with the MSI score of GC patients. (D) The correlation analysis of *CCDC6* expression with OS of GC patients was conducted with Kaplan-Meier plotter. (E–H) Correlation analyses of *CCDC6* expression with OS of GC patients with stage I, stage II, stage III, or stage IV disease. (I) Correlation analysis of *CCDC6* expression with survival after chemotherapy in GC patients. GC patients were split into two groups with high and low expression of *CCDC6* based on the autoselected best cutoff provided by KM plotter.

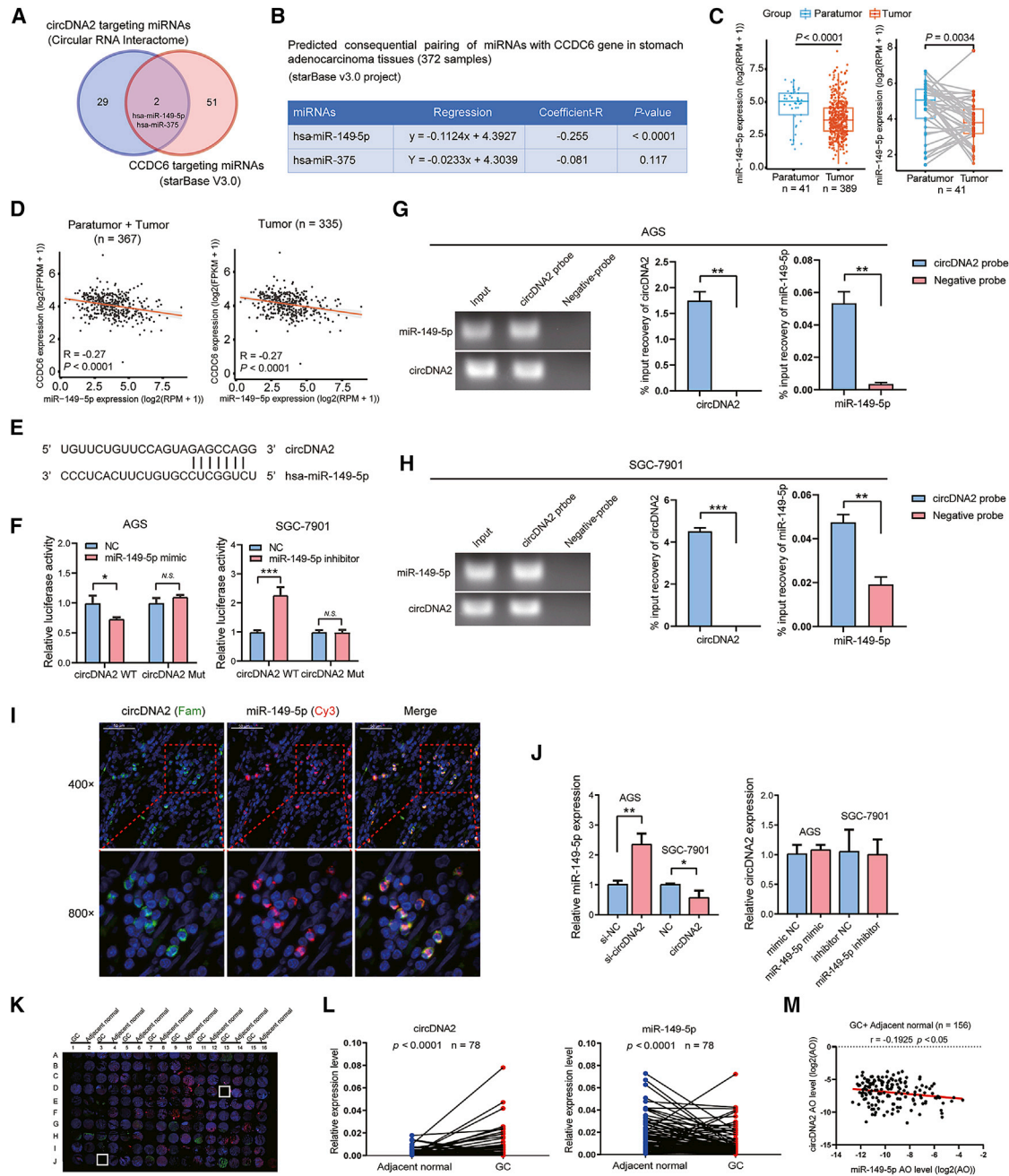


Figure 4. Identification of miR-149-5p as a potential miRNA for circDNA2 sponging

(A) We screened out hsa-miR-149-5p and hsa-miR-375, which can target the *CCDC6* gene 3' UTR and be sponged by circDNA2. (B) Predicted consequential pairing of miRNAs with the *CCDC6* gene in 372 GC tissues from TCGA database. (C) The relative expression levels of miR-149-5p in GC tissues and adjacent normal tissues were analyzed using TCGA RNA-seq data. (D) Pearson correlation analyses between miR-149-5p and *CCDC6* expression were performed for GC tissues and adjacent normal tissues using TCGA data. (E) The predicted binding site of circDNA2 and miR-149-5p. (F) Dual-luciferase reporter assays were used to determine whether there was a direct binding site between circDNA2 and miR-149-5p. (G and H) Coprecipitation and detection of circDNA2 and miR-149-5p in AGS and SGC-7901 cell lysates with RNA pulldown and quantitative real-time PCR assays. (I) FISH analysis revealed that circDNA2 colocalized with miR-149-5p in the cytoplasm of GC tissue cells. Scale bars, 50 μ m. (J) Mutual regulation of circDNA2 and miR-149-5p indicated by quantitative real-time PCR. (K) RNA FISH assays for a human GC tissue microarray. (L and M) The relative expression levels and correlation of circDNA2 and miR-149-5p in GC and pair-matched adjacent normal tissues. The data are represented as the mean \pm SEM. * $p < 0.05$, ** $p < 0.01$, *** $p < 0.001$.

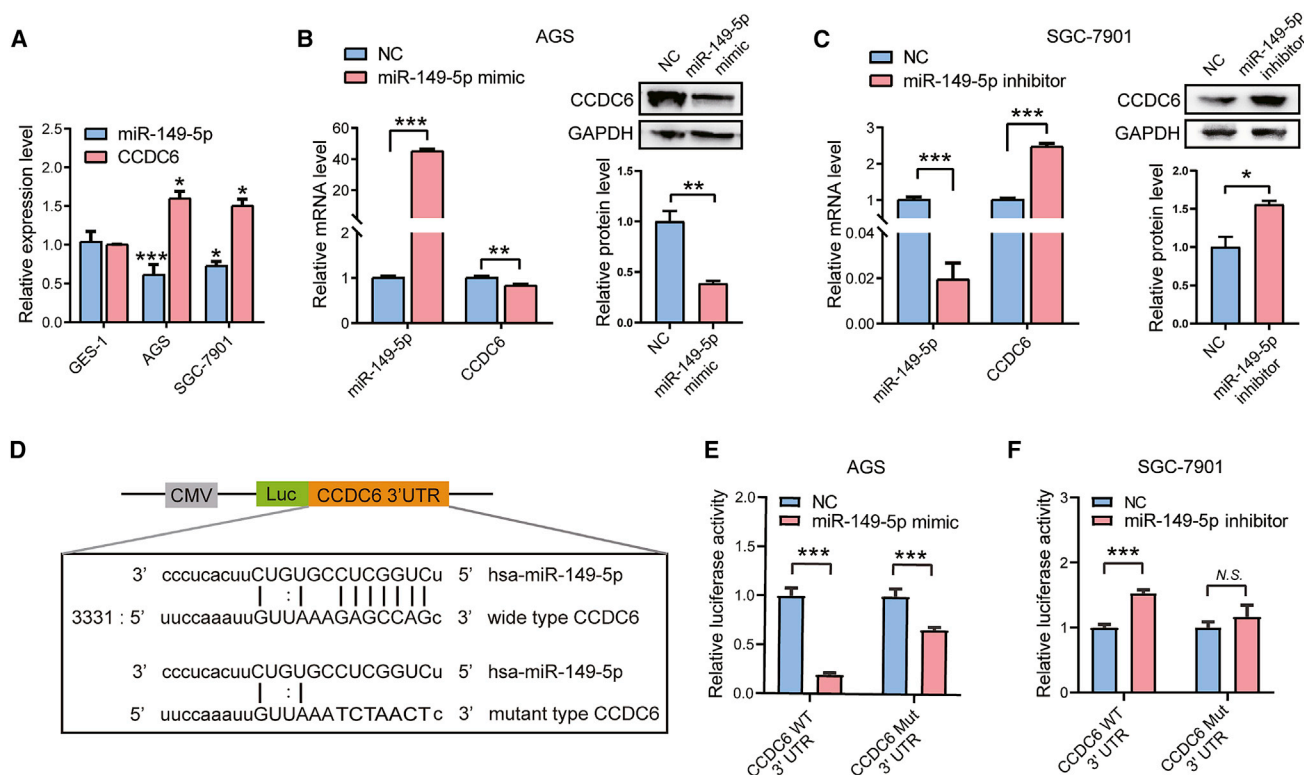


Figure 5. miR-149-5p was validated to target *CCDC6* gene

(A) The relative expression levels of miR-149-5p and *CCDC6* in GES-1 cells and AGS and SGC-7901 GC cells by quantitative real-time PCR detection. (B and C) The relative expression levels of miR-149-5p and *CCDC6* in AGS or SGC-7901 GC cells transfected with miR-149-5p mimic or inhibitor for 48 h by quantitative real-time PCR and western blot detection. (D) Schematic diagram of the binding sites of WT or Mut *CCDC6* 3' UTR and miR-149-5p. (E) The luciferase activity of AGS cells with cotransfection of WT or Mut *CCDC6* 3' UTR with miR-149-5p mimic. (F) The luciferase activity of SGC-7901 cells with cotransfection of WT or Mut *CCDC6* 3' UTR with miR-149-5p inhibitor. The data are represented as the mean \pm SEM. * $p < 0.05$, ** $p < 0.01$, *** $p < 0.001$.

RNA (siRNA) against the backspliced sequence of circDNA2 (Figure 6A) and detected their transfection efficiency in AGS and SGC-7901 GC cells (Figure 6B). We further determined that the *CCDC6* expression level in the circDNA2 transfection group was significantly strengthened compared with that in the NC group, while knockdown of circDNA2 with si-circDNA2 significantly decreased the level of *CCDC6* compared with that in the si-NC transfection group (Figure 6C). Since *CCDC6* was previously reported to promote tumor cell proliferation²⁹⁻³¹ and circDNA2 might enhance *CCDC6* expression by sponging miR-149-5p based on our aforementioned results, we therefore investigated whether circDNA2 affected GC cell proliferation by performing functional assays. As shown in Figures 6D–6F, the GC cell proliferative capacity was comprehensively evaluated by CCK-8, 5-ethynyl-2'-deoxyuridine (EdU), and colony formation assays. We found that AGS cell proliferation was inhibited by transfection of si-circDNA2, while circDNA2 overexpression enhanced SGC-7901 cell proliferation. Moreover, miR-149-5p knockdown recovered si-circDNA2-induced inhibition of AGS cell proliferation, and cotransfection of miR-149-5p mimics reversed the cell proliferation caused by circDNA2 in SGC-7901 cells.

circDNA2 and miR-149-5p expression were associated with lymphatic invasion and prognosis of GC patients, respectively

We first evaluated whether circDNA2 and miR-149-5p expression were correlated with the clinicopathological characteristics and prognosis of 78 GC patients. circDNA2 expression was positively associated with lymph node metastasis in the GC patients (N0 + N1 versus N2 + N3, $p = 0.0124$). In addition, circDNA2 and miR-149-5p were not significantly correlated with other clinical parameters of the GC patients ($p > 0.05$; Figures 7A and 7B; Tables S1 and S2). The expression levels of circDNA2 and miR-149-5p in GC tissues and adjacent normal tissues were divided into two groups, high expression and low expression, and binary logistic regression analysis was used to construct a risk score for the incidence of GC (Figure 7C). The area under the curve (AUC) for circDNA2 combined with miR-149-5p to assess the GC occurrence rate was 0.7301 (sensitivity 61.5%, specificity 79.5%), suggesting that circDNA2 and miR-149-5p may be biomarkers for predicting GC occurrence.

Furthermore, we did not find that the circDNA2 expression level was significantly correlated with OS or survival after chemotherapy in the GC patients (Figures S3A–S3D and S3G). GC patients with low

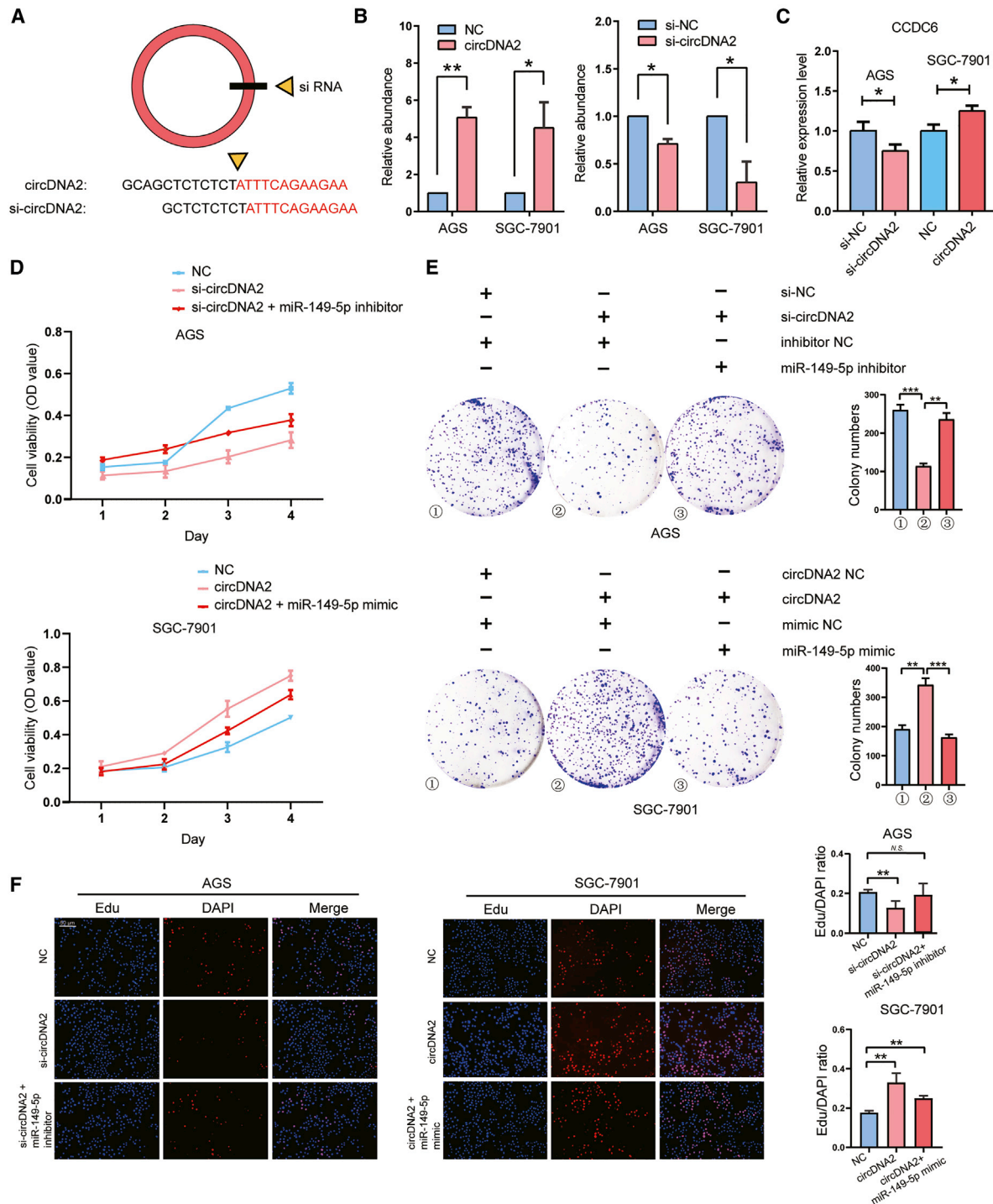


Figure 6. Knockdown of circDNA2 reduced *CCDC6* expression and inhibited the proliferation of GC cells *in vitro*

(A) Schematic diagram of the siRNA sequence for the backsplicing junction site of circDNA2. (B) The transfection efficiency was detected by quantitative real-time PCR assays 48 h after transfection of the overexpression plasmid or the siRNA of circDNA2. (C) The *CCDC6* level was determined by quantitative real-time PCR assays in the circDNA2 or si-circDNA2 transfection group relative to the corresponding NC transfection group. (D–F) Cell proliferation of AGS and SGC-7901 GC cells transfected with circDNA2 knockdown or overexpression was comprehensively evaluated by CCK-8, EdU, and colony formation experiments; scale bar, 50 μ m. The data are represented as the mean \pm SEM. * $p < 0.05$, ** $p < 0.01$, *** $p < 0.001$.

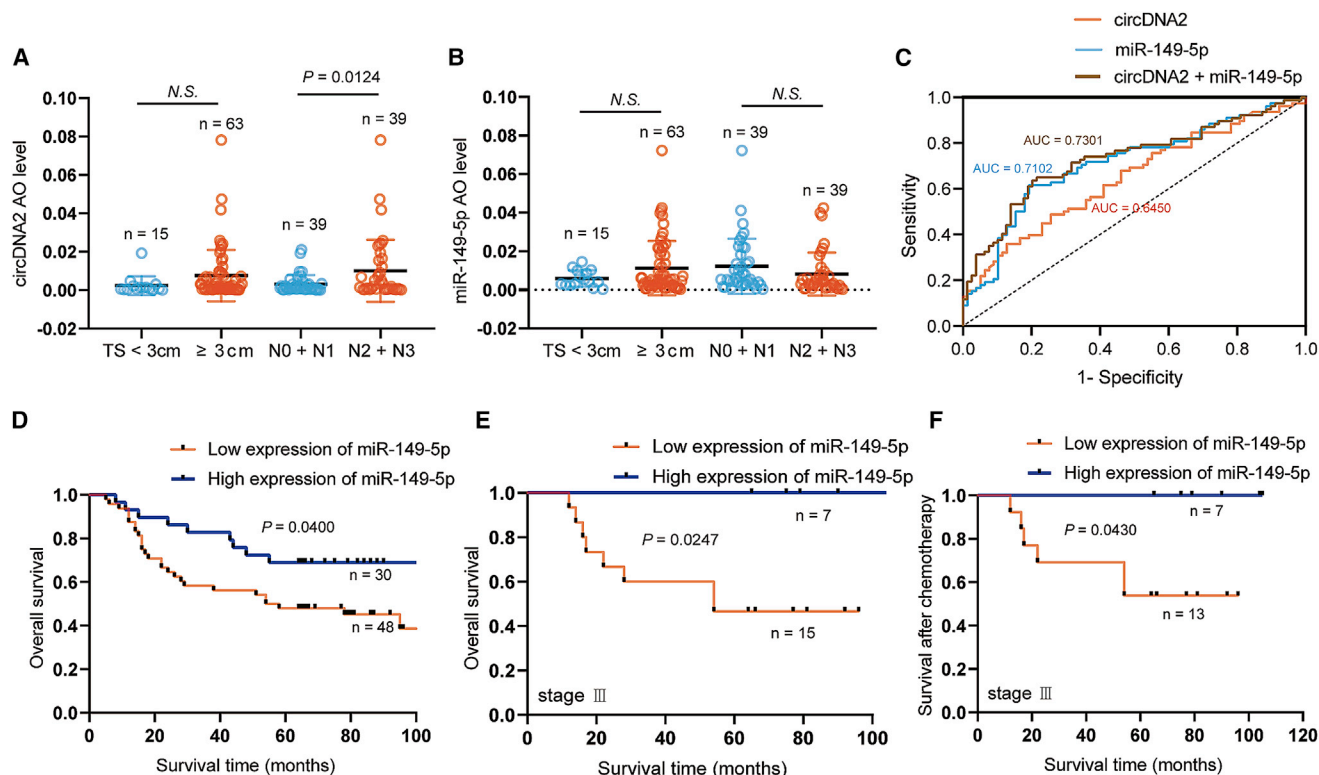


Figure 7. circDNA2 and miR-149-5p levels were associated with lymph node metastasis and prognosis of GC patients

(A and B) Correlations of the AO levels of circDNA2 or miR-149-5p with tumor size (TS) or lymph node metastasis. (C) circDNA2 and/or miR-149-5p were included to construct a risk score for GC incidence using binary logistic regression analysis. The circDNA2 cutoff value was 0.001120856 (MaxSpSe: maximizes sensitivity and specificity simultaneously), and miR-149-5p cutoff value was 0.006809315 (Youden index). (D) The correlation of miR-149-5p expression levels with the OS of GC patients. (E and F) The correlation of miR-149-5p expression level with (E) OS and (F) survival after chemotherapy of GC patients with stage III disease. The cutoff value of miR-149-5p expression levels was based on the Youden index.

miR-149-5p expression had a shorter OS than GC patients with high miR-149-5p expression (Figure 7D). Further pathological staging analysis revealed that GC patients with stage III disease with low miR-149-5p expression had significantly poorer OS and survival after chemotherapy (Figures 7E and 7F; Figures S3E, S3F, and S3H).

DISCUSSION

For the current study, we aimed to investigate whether *CCDC6* expression in GC tissues and cell lines was regulated by ncRNAs, similar to the other tumor types mentioned above. First, we filtered out highly expressed circDNA2 in GC tissues from our RNA-seq results and further determined that circDNA2 existed stably in the cytoplasm because of its circular structure. Second, we discovered that circDNA2 knockdown obstructed proliferation and *CCDC6* expression in GC cells, whereas miR-149-5p inhibition reversed the effects of circDNA2 knockdown and promoted GC cell proliferation. Additionally, GC patients with high expression of circDNA2 often had lymph node metastasis, indicating the progression of GC. Although we found that a consistent trend was observed in *CCDC6* expression when the expression of circDNA2 was inhibited or promoted in GC

cells (Figure 6C), circDNA2 in the cytoplasm did not directly affect the transcriptional process of the *CCDC6* gene.

Considering that circRNAs act as miRNA sponges to play a post-transcriptional role in a variety of tumors³² and sequestering a miRNA may diminish its repressive effects on its target genes,³³ miR-149-5p targeting of the *CCDC6* gene was confirmed through bioinformatics analyses, which showed that this miRNA was also sponged by circDNA2. We next demonstrated that miR-149-5p directly bound to *CCDC6* or circDNA2 via dual-luciferase reporter gene assays and functional gain and loss experiments. Several studies^{20,34,35} independently reported that miR-149-5p has a tumor-suppressive role in GC, which was consistent with our findings. In our study, the AUC for a single miR-149-5p expression level to predict the risk of GC occurrence reached 0.7102, indicating that miR-149-5p has potential as a biomarker for GC diagnosis. In addition, low expression of miR-149-5p might indicate a potentially poor prognosis for GC patients with shortened OS and survival after chemotherapy.

Previous studies on *CCDC6*-related oncology have focused on the thyroid, liver, and lung. *CCDC6* was identified as the target gene of

miR-146-5p in PTC¹⁶ and miR-19b-3p in intrahepatic cholangiocarcinoma (ICC)¹⁹ and inhibited cell proliferation and epithelial-mesenchymal transition and facilitated cell apoptosis. However, the fusion of the *RET* kinase with its partner protein *CCDC6* led to cell proliferation by activating downstream intracellular signaling and enhancing gene transcription in non-small cell lung cancer.^{29,30} For instance, LC-2/ad cells are a human lung adenocarcinoma cell line endogenously expressing the *CCDC6-RET* fusion gene, which contributes to ERK1/2 phosphorylation and cell proliferation in a xenograft model.³¹ In this study, we explored the expression of *CCDC6* in GC patients and its association with the clinicopathological characteristics and prognosis of GC patients, which suggested that *CCDC6* was highly expressed in GC tissues relative to adjacent normal gastric tissues, and GC patients with high *CCDC6* expression possessed high levels of MSI and shortened OS and survival after chemotherapy. Our results might help elucidate the roles of *CCDC6* in the pathogenesis of GC.

Our RNA-seq data revealed that the predicted sequence length of 83.62% of the circRNAs was <1,000 nucleotides (Figure 1B), which was similar to previously published literature.²⁰ However, we found that 95.96% of the circRNAs were derived from exons (Figure 1C), while Zhang X et al. reported that 56.57% of circRNAs were derived from introns. This difference in the gene distribution of circRNAs might be because the abovementioned literature analyzed the total circRNAs detected (n = 35,156), while we analyzed the circRNAs that could be annotated on the circBase website (n = 3,120).

In summary, circDNA2 and miR-149-5p both have potential to be developed as biomarkers for the diagnosis of GC. The advantage of circDNA2 as a biomarker is that it has a stable loop structure, while the advantage of miR-149-5p is that it can also predict OS and survival after chemotherapy in GC patients. In this study, we also revealed that *CCDC6* is a novel target in GC tumorigenesis that is associated with MSI and unfavorable prognosis of GC patients and should be further explored to elucidate its underlying mechanisms.

MATERIALS AND METHODS

Patient samples

The clinicopathological data of GC cases and the relative expression levels of the *CCDC6* gene and miRNAs, including hsa-miR-149-5p, hsa-miR-654-3p, and hsa-miR-375, in GC tissues were obtained from the TCGA 2015 RNA-seq database (<http://xena.ucsc.edu/getting-started/>). A human tissue microarray containing 80 pairs of GC tissues and matched adjacent normal gastric tissues (Cat No. STC1602) was acquired from Shanghai Superbiotech Pharmaceutical Technology Co., Ltd. (Shanghai, China). Twenty pairs of GC and adjacent normal gastric tissues were immediately collected after surgical resection from the First Affiliated Hospital of Nanjing Medical University in 2019 and used to compare the relative expression of *CCDC6* between tumor and adjacent tissues. The study protocols were approved by the Ethical Committee of the First Affiliated Hospital of Nanjing Medical University.

RNA sequencing

Three pairs of GC tissues were randomly selected for RNA-seq from the abovementioned 20 pairs of GC tissues collected by our center. Relevant clinicopathological details of the 3 selected GC patients are listed in Table S4. After the ribosomal RNAs were removed from total RNA with Ribo-Zero rRNA Removal Kits (Illumina, USA), RNA-seq libraries were constructed by using a TruSeq Stranded Total RNA Library Prep Kit (Illumina, USA) and further controlled for quality and quantified with the BioAnalyzer 2100 system (Agilent Technologies, USA). Ten pM libraries were denatured as single-stranded DNA molecules, captured on Illumina flow cells, amplified *in situ* as clusters, and finally sequenced for 150 cycles on an Illumina HiSeq 4000 Sequencer. Q30 was used for quality control of paired-end reads, and Cutadapt software (v.1.9.3) was used for trimming the 3' adaptor and removing low-quality reads. Finally, circRNAs were analyzed with high-quality trimmed reads.

Identification of differentially expressed circRNAs

RNA-seq reads were aligned to the reference genome UCSC HG19 with Bowtie2 software, and circRNAs were detected and identified with find_circ software. The identified circRNAs were annotated with circBase and circ2Traits databases. Raw junction reads for all samples were normalized by total read number and log₂ transformed. Differentially expressed circRNAs (fold-change cutoff > 2, p < 0.05) were identified by t tests between GC tissues and adjacent normal tissues.

Cell culture

The human normal gastric epithelial cell line GES-1 and GC cell lines AGS, SGC-7901, and BGC-823 were maintained by the Institute of Digestive Diseases of the First Affiliated Hospital of Nanjing Medical University. All cells were cultured in RPMI 1640 medium supplemented with 10% fetal bovine serum (FBS) and 1% penicillin-streptomycin solution (Beyotime, Haimen, China) and placed in a humidified incubator containing 5% CO₂ at 37°C.

RNA extraction and quantitative real-time PCR

Total RNA of GC cells or tissues was extracted by TRIzol reagent (Invitrogen, Carlsbad, CA, USA). The minimum number of GC cells required for total RNA extraction was $\sim 2.5 \times 10^5$ cells. NE-PER Nuclear and Cytoplasmic Extraction Reagents (Thermo Fisher Scientific, Waltham, MA, USA) were used to separate cytoplasmic and nuclear RNA fractions. Reverse transcription of mRNAs and circRNAs was performed with SuperScript II (TaKaRa, Dalian, China), and quantitative real-time PCR was performed with a SYBR Green Master Mix kit (TaKaRa). Reverse transcription for miRNAs was implemented with a PrimeScript RT reagent Kit (TaKaRa) following the manufacturer's instructions. Each sample was reverse transcribed with 1,000 ng of RNA. Sequences of the PCR primers are listed in Table S3. Bulge-loop miRNA quantitative real-time PCR Primer Sets (one RT primer and a pair of qPCR primers) specific for miR-149-5p were designed by RiboBio (Guangzhou, China). *GAPDH* was used as the internal reference for mRNA and circRNA. The miRNA level was normalized to the *RNU6-1* level.

RNase R and actinomycin D treatment

Total RNA was digested by 3 U/mg RNase R exonuclease (Epicenter Technologies, Madison, WI, USA) for 20 min at 37°C to degrade linear RNA. Total RNA was harvested after addition of 2 mg/mL actinomycin D (Sigma-Aldrich, St. Louis, MO, USA) to inhibit transcription. Reverse transcription and quantitative real-time PCR were then performed on RNase R- or actinomycin D-treated RNA.

RNA fluorescence *in situ* hybridization

Both GC and adjacent normal gastric tissues fixed in 4% paraformaldehyde were embedded in paraffin and then sectioned. The sections were gradually dewaxed in xylene and 100%, 85%, and 75% ethanol for subsequent FISH experiments. circDNA2 probe sequence: 5'-DIG-CTTTCTTCTGAAATAGAGAGAGCTGCATCT-DIG-3'; miR-149-5p probe sequence: 5'-CY3-GGGAGTGAAGACACGGAGCCAGA-3'. The sections were hybridized with 6 ng/ μ L of digoxigenin (DIG)-labeled circDNA2 probe overnight at 37°C and then washed with saline sodium citrate (SSC) and 50% formamide to remove hybridization buffer. The sections were incubated with anti-DIG-horse radish peroxidase (HRP) (Jackson ImmunoResearch, Inc., West Grove, PA, USA) at 4°C for 50 min and then washed three times in PBS for 5 min each time. Subsequently, the sections were incubated with fluorescein isothiocyanate (FITC)-TSA (Servicebio, Wuhan, China) to amplify the fluorescent signal. The miR-149-5p probe (8 ng/ μ L) was also added to the slices for hybridization at 37°C overnight to observe whether circDNA2 and miR-149-5p were colocalized in the cytoplasm of GC tissue cells. The nuclei were stained with DAPI and incubated in the dark for 8 min. Images were captured under a Nikon upright fluorescence microscope. Image-Pro Plus 6.0 (Media Cybernetics, Inc., Rockville, MD, USA) software was used to analyze the green/red fluorescence monochrome photos to obtain the average optical density (AO) of each photo, which represented the positive expression levels of circDNA2 and miR-149-5p.

Luciferase reporter assay

The 3' UTR sequence of circDNA2 was cloned into a pGL3 promoter. AGS and SGC-7901 cells were seeded in 24-well plates for 24 h and then cotransfected with miR-149-5p mimic or inhibitor and NC with the WT or Mut 3' UTR of circDNA2. In addition, WT or Mut CCDC6 3' UTR was cotransfected with miR-149-5p mimic or inhibitor in AGS or SGC-7901 cells. After 48 h of transfection, firefly luciferase activities were detected with a dual-luciferase reporter kit (Promega, Madison, WI, USA) and further normalized to *Renilla* luciferase activities.

circRNA pulldown assay

The biotinylated circDNA2 probe was specifically designed to bind to the junction region of circDNA2 (biotin-labeled circDNA2 probe: 5'-CCACTTTCTTCTGAAATAGAGAGAGCTGCATCTG-3'), while the scramble 22 nt oligo probe was used as a control (biotin-labeled negative probe: 5'-GTGTAACACGTCTATACGCCCA-3'). Approximately 6×10^7 cells were harvested and lysed. The circDNA2-specific probe was incubated with streptavidin magnetic beads (Thermo Fisher, USA) at 4°C overnight to generate probe-coated beads. The

cell lysates were incubated with probe-coated beads at room temperature for 1 h. The beads were washed, and the bound miRNAs in the pulldown samples were extracted with TRIzol reagent and further evaluated by quantitative real-time PCR assays.

Plasmid and oligonucleotide transfection

Plasmid and siRNA vectors targeting circDNA2 and miR-149-5p mimic or inhibitor were commercially obtained from GenePharma (Shanghai, China). si-DNA2 sequence: 5'-GCTCTCTCTATTTCA GAAGAA-3'. The human GC cell lines AGS and SGC-7901 were seeded in 6-well plates to reach 80%–90% confluence and then transfected with circDNA2 overexpression plasmid, si-circDNA2, and miR-149-5p mimic or inhibitor accompanied by Lipofectamine 2000 (Invitrogen, Carlsbad, CA, USA) for 48 h.

Western blot

Protein extracts were boiled with loading buffer and then separated by electrophoresis on 10% SDS-PAGE gels. After transfer onto a polyvinylidene fluoride (PVDF) membrane, separated protein bands were blocked with bovine serum albumin (BSA) for 1 h. The PVDF membranes were hybridized with the primary antibodies overnight at 4°C and then immunoblotted with a corresponding HRP-labeled secondary antibody for 1 h at room temperature. The primary antibodies against CCDC6 (cat. 13717-1-AP, Proteintech, Wuhan, China) and GAPDH (cat. AF5009, Beyotime, Shanghai, China) were diluted according to the recommended ratio, while the secondary antibodies were diluted at a ratio of 1:10,000. Blot signals were visualized with HRP substrate (WBKL0100, Millipore, USA) and captured by a Bio-Rad ChemiDoc XRS+ imaging system. The band images were quantified by a densitometry with ImageJ software, followed by normalization to the loading control GAPDH.

CCK-8 assay

The proliferative activities of AGS and SGC-7901 GC cells were identified by a Cell Counting Kit-8 assay (Dojindo Laboratories, Kumamoto, Japan). Briefly, GC cells were plated in 96-well plates (3,000 cells per well) and incubated with 10 μ L of CCK-8 solution per well for 1 h on days 1, 2, 3, and 4. The absorbance of the test wells at 450 nm was measured for analysis.

Colony formation assay

AGS and SGC-7901 GC cells were seeded in 6-well plates (800 cells per well). After incubation at 37°C for 2 weeks, the cell colonies were fixed with 4% paraformaldehyde for 20 min and then stained with 0.1% crystal violet for 20 min. All plates were photographed, and the cell colonies were counted for analysis.

EdU assay

The proliferation of the treated AGS and SGC-7901 GC cells was monitored by an EdU Cell Proliferation Kit (RiboBio, Guangzhou, China). GC cells were seeded in 96-well plates at a density of 1×10^4 cells per well overnight. EdU solution (50 μ M) was added to each well of the test plate and incubated with cells for 2 h. The GC cells were then fixed with 4% formaldehyde for 30 min and

subsequently permeabilized with 0.5% Triton X-100 for 10 min. Apollo dye solution (200 μ L) and Hoechst 33342 (200 μ L) were added to stain the EdU-stained cells and the nucleic acids in the cells, respectively. Images were captured to calculate the percentage of EdU-positive GC cells.

Statistical analysis

IBM SPSS Statistics 23.0 and GraphPad Prism 8.0 software were used for statistical analyses. Student's *t* test or chi-square test was applied to compare two groups. Comparisons of paired samples were performed by paired *t* test analysis. Pearson's correlation coefficient was calculated to evaluate the correlations. OS curves were obtained from the Kaplan-Meier plotter with a log-rank *p* value. Spearman's correlation analysis was used to describe the correlation between two quantitative variables without a normal distribution with R v.4.0.3 software. In this study, we revealed the correlation of CCDC6 gene expression levels with the MSI score of GC patients. Cell experiments were performed in triplicate, and all results are presented as the mean \pm the standard error of the mean. *p* < 0.05 was considered significant.

SUPPLEMENTAL INFORMATION

Supplemental information can be found online at <https://doi.org/10.1016/j.omtn.2021.05.021>.

ACKNOWLEDGMENTS

This study was supported in part by the National Natural Science Foundation of China (no. 81770561 and no. 81970499) and the Jiangsu Province Leading Talents and Innovation Team (CXTDA2017033).

AUTHOR CONTRIBUTIONS

D. Jin and K. Huang conducted the experiments and wrote the manuscript; L. Peng, P. Xu, and Y. Dang designed the experiments; J. Yang designed the primers; M. Chen, X. Zhu, and S. Wei collected the human tissue samples; J. Yan and G. Zhang revised the manuscript and provided experimental funding.

DECLARATION OF INTERESTS

The authors declare no competing interests.

REFERENCES

- Bray, F., Ferlay, J., Soerjomataram, I., Siegel, R.L., Torre, L.A., and Jemal, A. (2018). Global cancer statistics 2018: GLOBOCAN estimates of incidence and mortality worldwide for 36 cancers in 185 countries. *CA Cancer J. Clin.* *68*, 394–424.
- Chiurillo, M.A. (2015). Role of the Wnt/ β -catenin pathway in gastric cancer: An in-depth literature review. *World J. Exp. Med.* *5*, 84–102.
- Ajani, J.A., Bentrem, D.J., Besh, S., D'Amico, T.A., Das, P., Denlinger, C., Fakhri, M.G., Fuchs, C.S., Gerdes, H., Glasgow, R.E., et al.; National Comprehensive Cancer Network (2013). Gastric cancer, version 2.2013: featured updates to the NCCN Guidelines. *J. Natl. Compr. Canc. Netw.* *11*, 531–546.
- Salzman, J., Gawad, C., Wang, P.L., Lacayo, N., and Brown, P.O. (2012). Circular RNAs are the predominant transcript isoform from hundreds of human genes in diverse cell types. *PLoS ONE* *7*, e30733.
- Li, R., Jiang, J., Shi, H., Qian, H., Zhang, X., and Xu, W. (2020). CircRNA: a rising star in gastric cancer. *Cell. Mol. Life Sci.* *77*, 1661–1680.
- Sanger, H.L., Klotz, G., Riesner, D., Gross, H.J., and Kleinschmidt, A.K. (1976). Viroids are single-stranded covalently closed circular RNA molecules existing as highly base-paired rod-like structures. *Proc. Natl. Acad. Sci. USA* *73*, 3852–3856.
- Memczak, S., Jens, M., Elefsinioti, A., Torti, F., Krueger, J., Rybak, A., Maier, L., Mackowiak, S.D., Gregersen, L.H., Munschauer, M., et al. (2013). Circular RNAs are a large class of animal RNAs with regulatory potency. *Nature* *495*, 333–338.
- Zhao, Y., Alexandrov, P.N., Jaber, V., and Lukiw, W.J. (2016). Deficiency in the Ubiquitin Conjugating Enzyme UBE2A in Alzheimer's Disease (AD) is Linked to Deficits in a Natural Circular miRNA-7 Sponge (circRNA; ciRS-7). *Genes (Basel)* *7*, 116.
- Zhang, M., Huang, N., Yang, X., Luo, J., Yan, S., Xiao, F., Chen, W., Gao, X., Zhao, K., Zhou, H., et al. (2018). A novel protein encoded by the circular form of the SHPRH gene suppresses glioma tumorigenesis. *Oncogene* *37*, 1805–1814.
- Zhang, J., Liu, H., Hou, L., Wang, G., Zhang, R., Huang, Y., Chen, X., and Zhu, J. (2017). Circular RNA_LARP4 inhibits cell proliferation and invasion of gastric cancer by sponging miR-424-5p and regulating LATS1 expression. *Mol. Cancer* *16*, 151.
- Chen, Y., Yang, F., Fang, E., Xiao, W., Mei, H., Li, H., Li, D., Song, H., Wang, J., Hong, M., et al. (2019). Circular RNA circAGO2 drives cancer progression through facilitating HuR-repressed functions of AGO2-miRNA complexes. *Cell Death Differ.* *26*, 1346–1364.
- Fusco, A., Grieco, M., Santoro, M., Berlingieri, M.T., Pilotti, S., Pierotti, M.A., Della Porta, G., and Vecchio, G. (1987). A new oncogene in human thyroid papillary carcinomas and their lymph-nodal metastases. *Nature* *328*, 170–172.
- Cerrato, A., Merolla, F., Morra, F., and Celetti, A. (2018). CCDC6: the identity of a protein known to be partner in fusion. *Int. J. Cancer* *142*, 1300–1308.
- Le Rolle, A.F., Klempner, S.J., Garrett, C.R., Seery, T., Sanford, E.M., Balasubramanian, S., Ross, J.S., Stephens, P.J., Miller, V.A., Ali, S.M., and Chiu, V.K. (2015). Identification and characterization of RET fusions in advanced colorectal cancer. *Oncotarget* *6*, 28929–28937.
- Roskoski, R., Jr. (2017). ROS1 protein-tyrosine kinase inhibitors in the treatment of ROS1 fusion protein-driven non-small cell lung cancers. *Pharmacol. Res.* *121*, 202–212.
- Jia, M., Shi, Y., Li, Z., Lu, X., and Wang, J. (2019). MicroRNA-146b-5p as an oncomiR promotes papillary thyroid carcinoma development by targeting CCDC6. *Cancer Lett.* *443*, 145–156.
- Leone, V., Langella, C., Esposito, F., De Martino, M., Decaussin-Petrucci, M., Chiappetta, G., Bianco, A., and Fusco, A. (2015). miR-130b-3p Upregulation Contributes to the Development of Thyroid Adenomas Targeting CCDC6 Gene. *Eur. Thyroid J.* *4*, 213–221.
- Jazdzewski, K., Murray, E.L., Franssila, K., Jarzab, B., Schoenberg, D.R., and de la Chapelle, A. (2008). Common SNP in pre-miR-146a decreases mature miR expression and predisposes to papillary thyroid carcinoma. *Proc. Natl. Acad. Sci. USA* *105*, 7269–7274.
- Tang, Y., Yang, J., Wang, Y., Tang, Z., Liu, S., and Tang, Y. (2020). MiR-19b-3p facilitates the proliferation and epithelial-mesenchymal transition, and inhibits the apoptosis of intrahepatic cholangiocarcinoma by suppressing coiled-coil domain containing 6. *Arch. Biochem. Biophys.* *686*, 108367.
- Zhang, X., Wang, S., Wang, H., Cao, J., Huang, X., Chen, Z., Xu, P., Sun, G., Xu, J., Lv, J., and Xu, Z. (2019). Circular RNA circNRI1 acts as a microRNA-149-5p sponge to promote gastric cancer progression via the AKT1/mTOR pathway. *Mol. Cancer* *18*, 20.
- Nagy, Á., Lánckzy, A., Menyhárt, O., and Györfi, B. (2018). Validation of miRNA prognostic power in hepatocellular carcinoma using expression data of independent datasets. *Sci. Rep.* *8*, 9227.
- Shah, M.Y., Ferrajoli, A., Sood, A.K., Lopez-Berestein, G., and Calin, G.A. (2016). microRNA Therapeutics in Cancer - An Emerging Concept. *EBioMedicine* *12*, 34–42.
- Bartel, D.P. (2004). MicroRNAs: genomics, biogenesis, mechanism, and function. *Cell* *116*, 281–297.
- Li, J.H., Liu, S., Zhou, H., Qu, L.H., and Yang, J.H. (2014). starBase v2.0: decoding miRNA-ceRNA, miRNA-ncRNA and protein-RNA interaction networks from large-scale CLIP-Seq data. *Nucleic Acids Res.* *42*, D92–D97.

25. Paraskevopoulou, M.D., Georgakilas, G., Kostoulas, N., Vlachos, I.S., Vergoulis, T., Reczko, M., Filippidis, C., Dalamagas, T., and Hatzigeorgiou, A.G. (2013). DIANA-microT web server v5.0: service integration into miRNA functional analysis workflows. *Nucleic Acids Res.* *41*, W169, W73.
26. Kertesz, M., Lovino, N., Unnerstall, U., Gaul, U., and Segal, E. (2007). The role of site accessibility in microRNA target recognition. *Nat. Genet.* *39*, 1278–1284.
27. Qu, S., Yang, X., Li, X., Wang, J., Gao, Y., Shang, R., Sun, W., Dou, K., and Li, H. (2015). Circular RNA: A new star of noncoding RNAs. *Cancer Lett.* *365*, 141–148.
28. Dudekula, D.B., Panda, A.C., Grammatikakis, I., De, S., Abdelmohsen, K., and Gorospe, M. (2016). CircInteractome: A web tool for exploring circular RNAs and their interacting proteins and microRNAs. *RNA Biol.* *13*, 34–42.
29. O’Leary, C., Xu, W., Pavlakis, N., Richard, D., and O’Byrne, K. (2019). Rearranged During Transfection Fusions in Non-Small Cell Lung Cancer. *Cancers (Basel)* *11*, 620.
30. Stinchcombe, T.E. (2020). Current management of *RET* rearranged non-small cell lung cancer. *Ther. Adv. Med. Oncol.* *12*, 1758835920928634.
31. Suzuki, M., Makinoshima, H., Matsumoto, S., Suzuki, A., Mimaki, S., Matsushima, K., Yoh, K., Goto, K., Suzuki, Y., Ishii, G., et al. (2013). Identification of a lung adenocarcinoma cell line with *CCDC6-RET* fusion gene and the effect of *RET* inhibitors in vitro and in vivo. *Cancer Sci.* *104*, 896–903.
32. Lin, W., Liu, H., Tang, Y., Wei, Y., Wei, W., Zhang, L., and Chen, J. (2021). The development and controversy of competitive endogenous RNA hypothesis in non-coding genes. *Mol. Cell. Biochem.* *476*, 109–123.
33. Smillie, C.L., Sirey, T., and Ponting, C.P. (2018). Complexities of post-transcriptional regulation and the modeling of ceRNA crosstalk. *Crit. Rev. Biochem. Mol. Biol.* *53*, 231–245.
34. Hui, C., Tian, L., and He, X. (2020). Circular RNA circNHSL1 Contributes to Gastric Cancer Progression Through the miR-149-5p/YWHAZ Axis. *Cancer Manag. Res.* *12*, 7117–7130.
35. Wang, Z., Liu, X., Liu, X., and Niu, D. (2020). Long Non-Coding RNA BLACAT1 Promotes the Tumorigenesis of Gastric Cancer by Sponging microRNA-149-5p and Targeting KIF2A. *Cancer Manag. Res.* *12*, 6629–6640.